Materials Advances

ROYAL SOCIETY OF CHEMISTRY

PAPER

View Article Online
View Journal | View Issue

Cite this: *Mater. Adv.*, 2025, 6, 9243

Bridging the gap between performance and biocompatibility: non-toxic, multifunctional aliphatic photoinitiators based on α-ketoesters for lithography-based manufacturing applications

Antonella Fantoni,[abc] Judith Krauß,[b] Theresa Ammann,[b] Philipp Melchior,[d] Dieter Nees,[d] Martin Frauenlob,[b] Robert Liska[bc] and Stefan Baudis*[abc]

Photoinitiators (PIs) represent the key molecules within a photopolymerizable resin, due to their ability to generate the initiating species. However, the majority of state-of-the-art PIs comprise aromatic chromophores, known to produce cytotoxic photoproducts, whose migration out of the cured resin poses both environmental and human health threats. Herein, we present a set of multifunctional, aliphatic free radical photoinitiators based on the α-ketoester moiety, which exhibit low cytotoxicity even after irradiation. By systematically increasing the number of PI moieties, purely aliphatic molecules comprised of up to four radical-generating units have been synthesized. High miscibility in both organic and water-based formulations, combined with excellent photoreactivity and no discoloration upon irradiation with broadband (320–500 nm) and LED (385 nm) light sources, are demonstrated. The developed α-ketoester derivatives outperform the benchmark Norrish type II benzophenone/amine system and can be used for advanced applications, including UV-nanoimprint lithography as well as additive manufacturing technologies (DLP 3D printing).

Received 18th August 2025,
Accepted 22nd October 2025

DOI: 10.1039/d5ma00926j

rsc.li/materials-advances

1. Introduction

Over the last few decades, photopolymerization has emerged as an important technology in various application fields, including decorative and protective coatings,[1] tissue engineering,[2] dental materials,[3] or 3D printing.[4] Among all available methods, radical photopolymerization is most frequently used and benefits from its energy efficiency (curing at room temperature) and fast curing rates accompanied by a low environmental impact (volatile organic compound free, no solvents).[5] Within a photopolymerizable formulation, the photoinitiator (PI) plays a fundamental role, as it leads to the generation of the initiating species upon irradiation. Thereafter, the PI molecules undergo either a mono- (Norrish type I) or bimolecular (Norrish type II) reaction to generate the initiating radicals. In a type I system, the absorption of a photon and subsequent intersystem crossing (ISC) produces radicals from the triplet state *via* homolytic bond cleavage. By contrast, type II photoinitiators generate radicals *via* hydrogen abstraction or electron/proton transfer with a suitable co-initiator, most frequently tertiary amines, upon excitation by light.[6]

A significant drawback of commercialized type I and type II PIs is the use of aromatic (*e.g.*, benzoyl) chromophores that can generate a variety of toxic photodecomposition products (*e.g.*, benzaldehyde).[7] Subsequently, migration of these substances out of a polymerized material becomes hazardous for both the environment and human health. As a result, the use of evermore photoinitiators is getting limited or banned in the European Union. The frequently used benzophenone (BP) is known to act as an endocrine disruptor in mammals[8] and is suspected to induce cancer growth in rats.[9] Another prominent example includes diphenyl(2,4,6-trimethylbenzoyl)phosphine oxide (TPO), which was added to the candidate list of substances of very high concern by the European Chemical Agency (ECHA) and classified as a reprotoxic substance.[10] There is also evidence in the literature that derivatives of phosphine oxides show high cytotoxicity and should thus be avoided in biomedical applications.[11]

Therefore, industrial and scientific focus has increasingly shifted towards the development and use of safer and biocompatible photoinitiators that do not generate toxic decomposition products while maintaining sufficient photoreactivity. Recently, the group of Pang presented various coumarin-3-oxoacetic acid

[a] *Christian Doppler Laboratory for Advanced Polymers for Biomaterials and 3D Printing, Getreidemarkt 9, 1060 Vienna, Austria*
[b] *Institute of Applied Synthetic Chemistry, Technische Universität Wien, 1060 Vienna, Austria. E-mail: stefan.baudis@tuwien.ac.at*
[c] *Austrian Cluster for Tissue Regeneration, 1200 Vienna, Austria*
[d] *Joanneum Research Materials, Institute for Sensors, Photonics and Manufacturing Technologies, 8160 Graz, Austria*

methyl esters with high cell viability (>80% at 8.92 mM) in L929 cells with high photoreactivity in multifunctional acrylates.[12] Gao *et al.* studied carbazole chalcone glyoxylate oxime esters as Norrish type I PIs for free radical photopolymerization (FRP) at 405 nm and 450 nm that outperformed several benchmark PIs, including TPO, methyl benzoylformate and phenylbis-(2,4,6-trimethylbenzoyl)-phosphine oxide (BAPO).[13] Cytotoxicity assays conducted with human umbilical vein endothelial cells (HUVECs) revealed higher cell viability of the developed PIs (>100% at ≤25 μM) compared to BAPO. Yin and coworkers synthesized a TPO-derivative bearing 9,10-dihydro-9-oxa-10-phospha-phenanthrene-10-oxide motifs combining high photoinitiation efficiency in FRP with low-toxicity in murine C3H10 T1/2 mesenchymal cells. Compared to the state-of-the-art TPO, the modification led to enhanced proliferation and migration of the cells at a concentration of 50 μM.[14] Further improvements in cell viability of radical photoinitiators have been made by the Ortyl group, as they recently presented benzoin ketal-based PIs for FRP of acrylates and hydrogels that exhibited high cell survival rates (>70% at ≤0.01 mM) in Chinese hamster ovary cells[15] and show no genotoxicity in *Salmonella typhimurium* bacteria strains[16] and were successfully applied in additive manufacturing applications.

Additionally, various studies have substituted the aromatic with an aliphatic moiety, giving either phenyl glyoxylates[12,17,18] or acetophenones.[19,20] Combining these concepts has led to the development of purely aliphatic photoinitiators, namely α-ketoesters (Fig. 1).[21,22]

Interestingly, these aliphatic molecules show an absorption maximum of ~330 nm (n–π*), although the molar extinction coefficient is significantly reduced compared to aromatic substances (*e.g.*, phenyl glyoxylates).[21,22] The radical generation of aliphatic α-ketoesters has rarely been studied since the 1960s, indicating that radicals are generated after an intramolecular triplet-state hydrogen abstraction. Thereby, biradical intermediates are generated that allow for the initiation of the radical polymerization.[23,24] More specifically, the H-abstraction can occur on the aliphatic chain next to the ketone[25] (Fig. 2(A)) as well as on the aliphatic ester residue[26] (Fig. 2(B)) without the addition of a co-initiator.

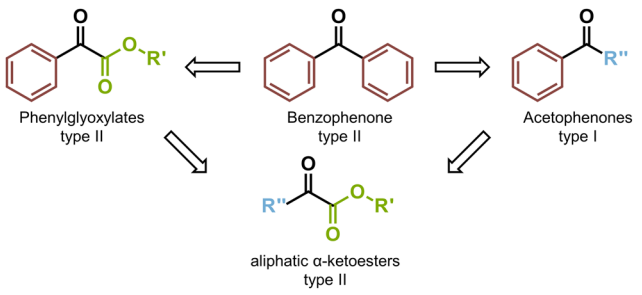

Fig. 1 Schematic pathway towards the step-wise substitution of the benzoyl moieties of benzophenone towards phenyl glyoxylates (left) and acetophenones (right). Combination of both approaches leads to the development of fully aliphatic α-ketoesters.

α-Ketoesters, as well as α-ketoacids and their decomposition products, are known for their excellent biocompatibility.[27–29] α-Ketoglutaric acid is a metabolite in the Krebs cycle and converted into α-ketoglutarate.[30] Therefore, it has been used as a radical PI for hydrogels.[31,32] Furthermore, the simplest α-ketoester, ethyl pyruvate, is an FDA-approved food additive with an LD_{50} value of >5000 mg kg^{-1} in Sprague–Dawley rats.[33] Recently, the photoreactivity of simple aliphatic (such as ethyl pyruvate) and macromolecular esters of ketoacids have been studied in (meth)acrylate resins as well as poly(ethylene glycol) (PEG) diacrylate-based hydrogels.[21,22] Therein, higher photoinitiation efficiency compared to benzophenone/amine systems was determined, as well as high biocompatibility with cell viabilities of >80% in L929 mouse fibroblasts before and after irradiation.

Nevertheless, the reports of using purely aliphatic photoinitiators are still limited. With this study, we aim to broaden the scope of currently available α-ketoester PIs. Herein, we present multifunctional PIs derived from abundantly available pyruvic acid and polyols (ethylene glycol, trimethylol propane, ethoxylated pentaerythritol) *via* straightforward synthetic methods. Thereafter, we characterized their UV-Vis absorbance and photoreactivity *via* photo differential scanning calorimetry (photo-DSC) in (meth)acrylates as well as acrylate-based hydrogels. Additionally, the cytotoxicity of the most promising PIs and their decomposition products was tested using L929 mouse fibroblasts. Finally, we applied purely aliphatic ketoesters as photoinitiators for nanoimprint lithography and DLP 3D printing.

2. Experimental

2.1. Materials and general methods

Ethyl pyruvate (KE1, TCI), trimethylolpropane (TMP, Sigma-Aldrich), ethylene glycol (EG, Sigma-Aldrich), ethoxylated pentaerythritol (15/4 EO/OH, M_n ~ 797 Da, Sigma-Aldrich), *N*,*N*′-dicyclohexylcarbodiimide (DCC, Fischer Scientific), benzophenone (BP, TCI), hexanediol diacrylate (HDDA, Roehm), ethoxylated trimethylolpropane triacrylate (14/3, 912 g mol^{-1}, TMPTA, Sigma-Aldrich), polyethylene diacrylate (PEGDA, M_n ~ 700 Da, used as a 50 wt% aqueous solution, Sigma-Aldrich), quinoline yellow (QY, Sigma-Aldrich), ethyl 4-dimethylaminobenzoate (EDB, Sigma-Aldrich), poly(ethylene glycol) (PEG, M_n ~1 kDa, Sigma-Aldrich), poly(propylene glycol) (PPG, M_n ~725 g mol^{-1}, Sigma-Aldrich) and 2-hydroxy-4′-(2-hydroxyethoxy)-2-methylpropiophenone (IC2959, Ciba) were purchased from the respective suppliers and used without further purification. 4-(Dimethylamino)pyridine (DMAP, TCI) was recrystallized from toluene, pyruvic acid (PA, Fischer Scientific), and methyldiethanolamine (MDEA, Fluka) were distilled before use. Urethane dimethacrylate (UDMA) and 1,10-decandiol dimethacrylate (D3MA) were kindly obtained from Ivoclar Vivadent AG and used as an equimolar mixture (DMM). Commercial-grade dichloromethane (DCM, Donau Chemie) was dried using a PureSolv system (Inert, Amesbury, MA).

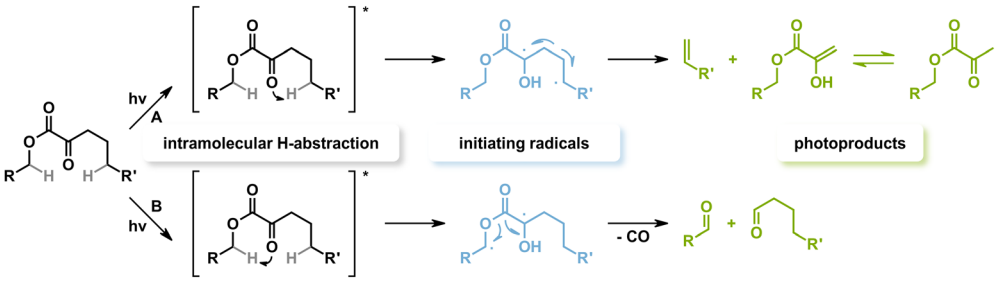

Fig. 2 Proposed Norrish type II mechanism of α-ketoesters by triplet-state absorption and subsequent radical generation *via* intramolecular H-abstraction on the side of the ketone (A) or on the side of the ester (B). The generated radicals (blue) initiate radical polymerization, thereafter photodecomposition gives alkenes and pyruvates, (A) whereas decarboxylation results in aldehydes or ketones (B).

Column chromatography was performed on a Büchi Sepacore flash system (Büchi pump module C-605, Büchi control unit C-620, Büchi UV-Photometer C-635, Büchi fraction collector C-660) using glass columns packed with silica gel (Merck, 0.040–0.063 mm). NMR spectra were recorded on a Bruker Avance DRX-400 FT-NMR spectrometer at 400 MHz for ^{1}H- and at 100 MHz for ^{13}C-spectra. The signals are reported with their chemical shifts in ppm and fine structure (s = singlet, d = doublet, t = triplet, q = quartet, qn = quintet, sep = septet, m = multiplet). The chemical shifts were referenced by using the respective NMR-solvent [^{1}H: $CDCl_3$ (7.26 ppm), ^{13}C: $CDCl_3$ (77.16 ppm)] as internal reference.

2.2. Synthesis of multifunctional photoinitiators

2.2.1. Synthesis of 2-(acetylcarbonyloxy)ethyl pyruvate (KE2). The synthesis of KE2 was conducted in a modified procedure from Gorsche *et al.*[34] A solution of ethylene glycol (2.00 g, 32.2 mmol, 1 eq.), pyruvic acid (5.96 g, 70.9 mmol, 2.2 eq.) and DMAP (0.32 g, 3.22 mmol, 0.1 eq.) in dry DCM (50 mL) was cooled to −10 °C. Thereafter, a solution of DCC (14.63 g, 70.9 mmol, 2.2 eq.) in dry DCM (90 mL) was added dropwise and stirred for two hours at 0 °C. Thereafter, the solution was warmed up to room temperature and stirred for 24 h. The formed precipitate was removed *via* filtration over silica gel, and the solution was concentrated *in vacuo*. The crude product was purified by column chromatography (113 g silica gel, petroleum ether/ethyl acetate 1 : 1) and precipitation of an insoluble by-product from cold (0 °C) ethyl acetate to give KE2 (2.08 g, 27%) as a colorless oil.

^{1}H NMR (400 MHz, $CDCl_3$) δ (ppm) 4.54 (s, 4H; –O–C$\underline{H}_2$–C$\underline{H}_2$–O–), 2.48 (s, 6H, –C$\underline{H}_3$) (Fig. S1).

^{13}C NMR (APT, 100 MHz, $CDCl_3$) δ (ppm) 191.1 (C═O), 160.5 (C═O), 63.4 (–O–$\underline{C}H_2$–$\underline{C}H_2$–O–), 26.9 (–$\underline{C}H_3$) (Fig. S2).

Elemental analysis: found: C, 46.5; H, 5.2; O. 48.9. calc. for $C_8H_{10}O_6$: C, 47.4; H, 5.0; O, 47.5%.

2.2.2. Synthesis of 2,2-bis[(acetylcarbonyloxy)methyl]butyl pyruvate (KE3). The synthesis of KE3 was conducted similar to KE2. In brief, a solution of TMP (2.00 g, 14.9 mmol, 1 eq.), pyruvic acid (4.33 g, 49.2 mmol, 3.3 eq.) and DMAP (0.44 g, 4.47 mmol, 0.3 eq.) in dry DCM (70 mL) was cooled to −10 °C. Thereafter, a solution of DCC (10.1 g, 49.2 mmol, 3.3 eq.) in dry DCM (100 mL) was added dropwise and stirred for two hours at 0 °C. Thereafter, the solution was warmed up to room temperature and stirred for 24 h. The formed precipitate was removed *via* filtration over silica gel, and the solution was concentrated *in vacuo*. The crude product was purified by column chromatography (213 g silica gel, petroleum ether/ethyl acetate 1 : 1) and precipitation of an insoluble by-product from cold (0 °C) ethyl acetate to give KE3 (1.42 g, 27%) as a colorless oil.

^{1}H NMR (400 MHz, $CDCl_3$) δ (ppm) 4.28 (s, 6H; –O–C$\underline{H}_2$–C–), 2.47 (s, 9H, –C$\underline{H}_3$), 1.58 (q, 2H, –C$\underline{H}_2$–CH$_3$), 0.94 (t, 3 H, –CH$_2$–C$\underline{H}_3$) (Fig. S3).

^{13}C NMR (APT, 100 MHz, $CDCl_3$) δ (ppm) 190.9 (C═O), 160.4 (C═O), 65.7 (–$\underline{C}H_3$), 41.6 (–C–), 26.8 (–O–$\underline{C}H_2$–), 23.3 (–$\underline{C}H_2$–CH$_3$), 7.5 (–CH$_2$–$\underline{C}H_3$) (Fig. S4).

Elemental analysis: found: C, 51.8; H, 6.1; O. 42.1. calc. for $C_{15}H_{20}O_9$: C, 52.3; H, 5.9; O, 41.8%.

2.2.3. Synthesis of ethoxylated pentaerythritol tetrapyruvate (KE4). The synthesis of KE4 was conducted similarly to KE2. Therefore, a solution of ethoxylated pentaerythritol (15/4 EO/OH, M_n ∼ 797 Da, 5.00 g, 6.27 mmol, 1 eq.), pyruvic acid (2.43 g, 27.6 mmol, 4.4 eq.) and DMAP (0.23 g, 1.88 mmol, 0.1 eq.) in dry DCM (50 mL) was cooled to −10 °C. Thereafter, a solution of DCC (5.71 g, 27.6 mmol, 4.4 eq.) in dry DCM (90 mL) was added dropwise and stirred for two hours at 0 °C. Thereafter, the solution was warmed up to room temperature and stirred for 48 h. The formed precipitate was removed *via* filtration, and the yellow solution was concentrated *in vacuo*. The crude product was dissolved in DCM (10 mL) and precipitated two-times into cold diethyl ether (−78 °C) to receive KE4 (4.34 g, 64%) as a highly viscous pale-yellow oil. To determine the conversion of free hydroxyl groups into pyruvate esters, quantitative ^{31}P-NMR[35] and gel permeation chromatography (GPC) were performed (Tables S1–S3). A conversion of 86% and a resulting M_n of ∼1480 Da were calculated.

^{1}H NMR (400 MHz, $CDCl_3$) δ (ppm): 4.41–4.38 (m, 8H, –CO–COO–C$\underline{H}_2$–), 3.79–3.77 (m, 8H, –CO–COO–CH$_2$–C$\underline{H}_2$–), 3.79–3.35 (m, 141H, –C$\underline{H}_2$– and –O–C$\underline{H}_2$–C$\underline{H}_2$–O), 2.47z (s, 12H, –C$\underline{H}_3$) (Fig. S5).

Elemental analysis: found: C, 52.2; H, 8.0; O, 38.7. calc. for $C_{47}H_{80}O_{27}$: C, 52.4; H, 7.5; O, 40.1%.

2.3. UV-Vis measurements

UV-Vis measurements of the synthesized KE2-3, as well as commercially available KE1 and BP, were conducted on a

Shimadzu UV-1800 photometer in scanning mode from 190–650 nm with a slit width of 2 nm. Analytes were used as 10^{-2} M solutions in HPLC-grade acetonitrile (Fischer Chemicals). The software Spectrum from PerkinElmer v10.03.07 was used to process the data.

2.4. Preparation of formulations

To ensure equal molar ratios of initiators to monomers, the monofunctional ethyl pyruvate (KE1) was used as a benchmark in a concentration of 2 mol%. All other initiators were used in equimolar amounts, relative to the amount of radical-generating moieties (*e.g.*, 1 mol% for difunctional KE2). For the ease of understanding, the molarity of PIs in monomers is given in functional group mol% (FG%). Methyldiethanolamine (MDEA) was used as a type II amine co-initiator in formulations with BP, as previous studies revealed that aliphatic ketoester PIs can be used as type II PIs without the addition of a co-inititiator.[21,22] For the investigation of the photoreactivity, the PIs were tested in various monomers, including HDDA or ethoxylated TMPTA as acrylate monomers, an equimolar mixture of UDMA and D3MA (DMM) as methacrylate monomers, and PEGDA ($M_n \sim 700$ g mol^{-1}) as a 50 wt% solution in water for hydrogels. To test the reactivity of KE3 in combination with MDEA, EDB, PEG, or PPG, equimolar amounts of co-initiators (with respect to KE3) were added. For PEG and PPG, equimolar ratios regarding the repeating unit of the polymers were used. The mixtures were thoroughly homogenized using a vortex mixer for 30 s. Thereafter, formulations were stored at 25 °C under light protection.

2.5. Photoreactivity by photo-DSC

The initiation performance of the PIs was evaluated using photo-differential scanning calorimetry (photo-DSC). The measurements were performed in triplicate on a Netzsch DSC 204 F1 equipped with an autosampler. For each measurement, 10 ± 2 mg of the respective formulation were placed in aluminum crucibles. A crucible with polymerized monomer was used as a reference. After an isothermal equilibrium phase of 240s, the samples were irradiated twice for 300 s with either filtered UV-light (320–500 nm) using an Exfo OmniCure™ series 2000 broadband Hg-lamp or a 365/385 nm LED (Omnicure Max LED heads in combination with a LX500 UV LED Spot Curing System) under constant N_2 flow rate (20 mL min^{-1}) at a light intensity of 40 mW cm^{-2} at the sample surface. The exothermic heat flow of the polymerization reaction was recorded as a function of time. Evaluation of the photo-DSC data was conducted using Proteus Thermal Analysis (version 5.2.1) from Netzsch. By integration of the peak area, the heat of polymerization ΔH_p was obtained. By comparing the theoretical heat of polymerization of the respective monomers (ΔH_0) with ΔH_p, the double bond conversion (DBC) was calculated according to eqn (1):

$$\mathrm{DBC}\,(\%) = 100 \times \frac{\Delta H_p}{f \cdot n \cdot \Delta H_0} \quad (1)$$

where ΔH_p is the measured heat of polymerization of the formulation in kJ mol^{-1}, ΔH_0 is the theoretical heat of polymerization of the formulation in kJ mol^{-1}, the factor f accounts for the molar proportion of the monomer in the formulation, and n is the number of polymerizable groups. The theoretical heat of polymerization for acrylates (80.5 kJ mol^{-1})[36] and DMM (58.5 kJ mol^{-1})[37] was indicated in the literature. For the hydrogels, f was adjusted to 0.5 to account for the 50 wt% aqueous formulation.

Additionally, the maximum rate of polymerization (R_p) was calculated following eqn (2):

$$R_p\left(\frac{\mathrm{mmol}}{\mathrm{L\ s}}\right) = \frac{h \cdot \rho}{n \cdot \Delta H_0} \quad (2)$$

where h is the height of the photo-DSC peak in mW mg^{-1}, ρ is the density of the formulation (ρ = 1010 g L^{-1} for HDDA, 1043 g L^{-1} for DMM and 1057 g L^{-1} for 50 wt% PEGDA in water), n is the number of polymerizable groups (= 2 for di(meth)acrylates) and ΔH_0 is the theoretical heat of polymerization of the formulation in kJ mol^{-1}.

Furthermore, the time until reaching the peak maximum (t_{max}) and the time until reaching 95% of the ΔH_p (t_{95}) were determined.

2.6. Evaluation of cytotoxicity

Mouse fibroblast cell line L929 was purchased from Sigma-Aldrich and cultured in Dulbecco's Modified Eagle's medium (Sigma Aldrich) supplemented with 10% fetal bovine serum (FBS, Sigma Aldrich) and 1% of antibiotic–antimycotic solution (100×, Sigma Aldrich). Cells were cultivated in a standard cell culture incubator in a saturated humid atmosphere with 5% CO_2 at 37 °C, medium was exchanged every two days, and cells were subcultivated in a 1 : 5 seeding ratio twice a week prior to experimental use in subcultivation passage 6. To evaluate the cytocompatibility of PIs, 96-well plates were seeded with 5000 cells per well and incubated overnight with complete medium (containing 10% FBS and 1% antibiotic–antimycotic solution). The following day, PIs were diluted in the respective amounts of DMEM without FBS and antibiotics and sterile-filtered to give the final concentrations of 17.84 mM, 8.93 mM, 4.46 mM, and 2.23 mM. The dilutions were added to the cells (100 µL per well, n = 8 biological replicates per concentration) without irradiation or after 10 min UV exposure in a UV Clave™ Ultraviolet Chamber (Benchmark, 254 nm, 500 µW cm^{-2}) and incubated for 24 hours at 37 °C and 5% CO_2. As control groups live (non-treated, only DMEM supplemented with FBS and antibiotics) and dead controls (exposure to 10% Triton-X in PBS) were included.

After 24 h incubation period with PIs, medium was exchanged twice with DMEM without FBS and antibiotics to remove PI residues and cell viability was evaluated by addition of 100 µL PrestoBlue™ solution diluted 1 : 10 in DMEM and incubated for 1 h at 37 °C, 5% CO_2. Fluorescence was then measured at 560 nm excitation and 590 nm emission wavelength with an EnSpire 2300 plate reader (PerkinElmer™). After

subtracting the background fluorescence and normalizing the data to the living control (cell viability 100%), the results of the cells exposed to different concentrations of PIs were evaluated using Origin Pro Version 2022b. Statistical evaluation was performed using One Way ANOVA Dunnett's Multiple Comparisons Test in GraphPad Prism 10.

2.7. UV-Nanoimprint lithography

Manual UV imprinting tests were performed with formulations containing 1 wt% KE3 in the respective monomer systems (NILcure bio-20, or M286/H_2O = 1/1; NILcure from JOANNEUM RESEARCH MATERIALS, M286 from MIWON). A droplet of formulation was placed on an anti-adhesion SAM-coated silicon master[38] and covered with PET (DuPont Teijin Films Melinex® ST505 Polyester Film d = 125 μm, for hydrogels) or cellulose hydrate (NatureFlex NP, d = 42 μm, BRC = 98%, for organic monomers) films. The resin/hydrogel precursor drop sandwiched between the Si-master and polymer substrate film gets readily spread by capillary forces. The formation of a thin uniform resin/hydrogel precursor film was further supported by applying slight pressure/rolling it out with a soft hand roller. Curing was performed by using a 365 nm LED lamp (JR self-built LED-array) at 100 mW cm^{-2} for 20 s through the transparent polymer film. Thereafter, the cured and structured polymer film adhered to the polymer substrate and was peeled off the Si master. The UV-nanoimprinted test structures were characterized by scanning electron microscopy (Raith eLiNE) after sputtering a thin gold layer on the imprinted structures.

2.8. DLP-3D printing

3D printing was conducted on a DLP 3D prototype printer (TU Wien, BP10) with an In-Vision Ikarus 2 light engine (max. intensity 75 mW cm^{-2}) with an irradiation wavelength of 385 nm. The building platform has a size of 42 × 38 mm^2 and a filling volume of 7.5 mL. Formulations (~3 mL) used for the 3D printing contained 2 FG% KE3 (in respect to ketoester moieties) in HDDA, ethoxylated trimethylolpropane triacrylate (TMPTA), or a hydrogel system consisting of 50 wt% PEGDA (M_n ~700 g mol^{-1}) in water. For TMPTA-based formulations, 0.02 wt% quinoline yellow was added as a UV absorber. For printing, the temperature of the building platform and vat were set to 25 °C. The first three base layers were irradiated with 65 mW cm^{-2} (15 s), while all other layers were irradiated for 10 s at 60 mW cm^{-2}. A layer thickness of 50 μm was chosen. After printing, the objects were removed with a blade, rinsed, and cleaned in an ultrasonic bath for 60 s with acetone or water (used for hydrogels). Visualization of printed parts was conducted by using a Keyence VHX6000 digital microscope with an objective that allows 20–2000× zoom. Scanning electron microscopy (SEM) images were obtained from a Zeiss EVO 10 device equipped with an Everhart-Thornley secondary electron detector and SmartSEM software. Before the imaging, the samples were sputtered with a thin gold layer and placed on a conductive carbon pad.

3. Results and discussion

3.1. Design of multifunctional α-ketoesters

Photoinitiators (PIs) based on the α-ketoester moiety generate radicals *via* intramolecular H-abstraction from the excited triplet state (Fig. 2).[21] Recently, our group showed that both low-molecular weight (cyclo-)aliphatic as well as polymerizable, high-molecular weight α-(poly)ketoesters enabled fast photopolymerization of (meth)acrylate resins.[21,22] However, excess of low-molecular weight PIs tend to leach out of a cured specimen, whereas polymeric PIs show lower migration tendencies, although accompanied with decreased photoreactivity resulting from the lower radical mobility. Therefore, we designed a yet unexplored class of α-ketoester-derived PIs, namely multifunctional α-ketoesters. Generally, multifunctional PIs are known to have high practical efficiency, low postcuring odor, and exhibit low migration tendency of the photolysis products.[39] Herein, the α-ketoester moiety should be attached to simple polyols to generate multifunctional PIs. We chose to start with ethyl pyruvate (KE1) as a commercially available, monofunctional PI. To obtain multifunctional PIs, ethylene glycol (KE2), trimethylol propane (KE3), and ethoxylated pentaerythritol (KE4) were modified with 2–4 pyruvate esters *via* Steglich esterification (Fig. 3).

By doing so, crowded α-ketoesters are generated that are no longer restricted to generate radicals within a linear chain (Fig. 4(A) and Fig. S7), but can harness from H-abstraction over the ''arms'' of the multifunctional PIs (Fig. 4(A)). Of course, KE1 and KE2 are limited in this cross-chain H-abstraction, whereas the spatial proximity of the ''arms'' in KE3 should enable H-abstraction on adjacent pyruvate groups. In the case of KE4, we additionally provided ethoxylated spacers to explore whether cross-chain H-abstraction also works with long, non-crowded side-chains.

3.2. Spectroscopic characterization of multifunctional α-ketoesters

The absorption behavior of KE1–4 was recorded *via* UV-Vis measurements in acetonitrile (1 × 10^{-2} M). Thereby, the n–π* transition and the corresponding molar extinction coefficient ε were determined on the maximum and for specific wavelengths (365, 385, 405 nm) and compared to benzophenone (BP) as Norrish type II reference (Table 1).

Previously, Gauss *et al.* reported the n–π* transition of simple α-ketoesters (including KE1) at around 330 nm,[21] which corresponds to the values determined for KE2–KE4 (329 nm). Interestingly, BP shows only slightly enhanced λ_{max}, (339 nm), even though the ketoesters lack an aromatic chromophore. As expected, we observed an increase in the molar extinction coefficient ε by increasing the amount of ketoester moieties per molecule. Thus, KE2 (30.9 M cm^{-1}) shows a 2-fold increase in $\varepsilon_{\lambda_{max}}$ compared to KE1 (16.9 M cm^{-1}), and following the same trend, KE3 and KE4 show a 3-fold (46.8 M cm^{-1}) and 4-fold (67.7 M cm^{-1}) increase, respectively. Similar behavior was observed for ε for all other wavelengths.

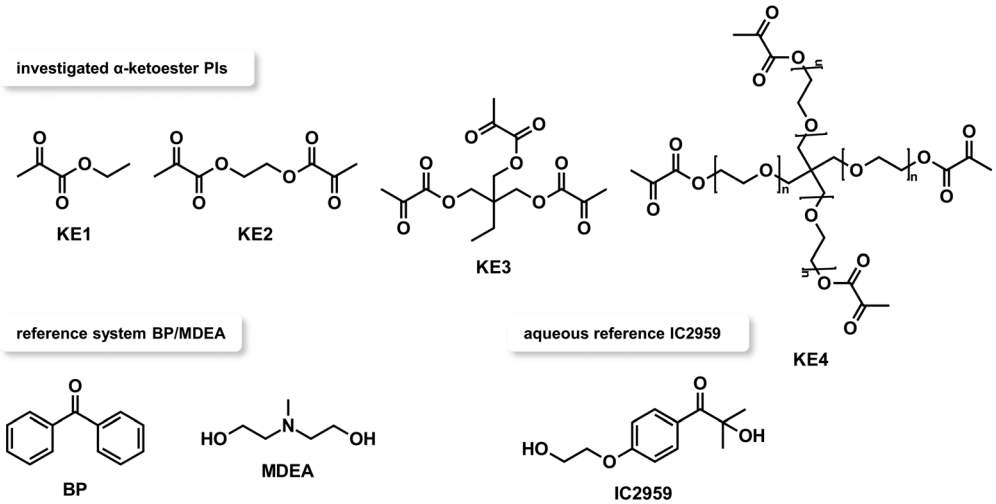

Fig. 3 Schematic representation of the photoinitiators: ethyl pyruvate (KE1), ethylene glycol dipyruvate (KE2), trimethylol propane tripyruvate (KE3), and ethoxylated pentaerythritol tetrapyruvate (KE4). The reference system for bulk (meth)acrylates consists of benzophenone (BP) and methyldiethanolamine (MDEA), whereas Irgacure 2959 (IC2959) was used as a reference in aqueous systems.

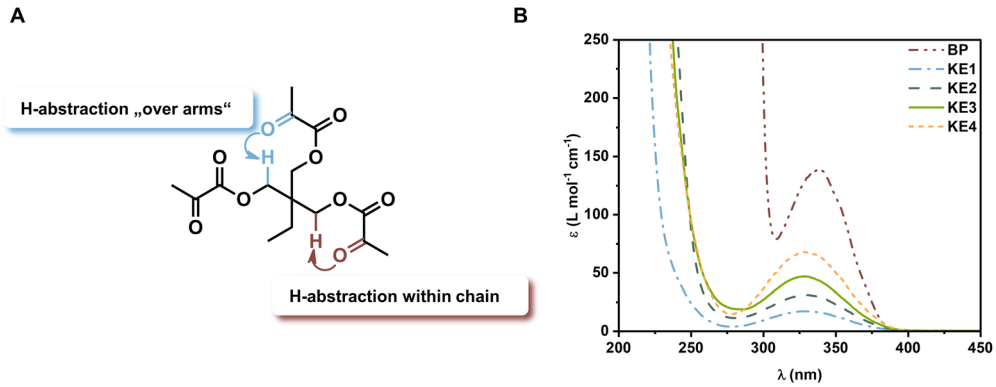

Fig. 4 (A) Proposed H-abstraction within the multifunctional α-ketoester KE3: "traditional" H-abstraction within the same chain (red) and over the arms of the core molecule (blue). (B) UV-Vis spectra of the reference BP and ketoesters KE1–KE4 in acetonitrile (1×10^{-2} M).

Table 1 Absorption properties of BP and KE1–KE4 in acetonitrile (1×10^{-2} M)

	λ_{max} (nm)	$\varepsilon_{\lambda_{max}}$ (L mol^{-1} cm^{-1})	ε_{365} (L mol^{-1} cm^{-1})	ε_{385} (L mol^{-1} cm^{-1})	ε_{405} (L mol^{-1} cm^{-1})
BP	339	138	57.2	4.20	0.30
KE1	329	16.9	6.67	1.29	0.10
KE2	329	30.9	12.4	2.70	0.20
KE3	329	46.8	17.2	3.50	0.40
KE4	329	67.7	26.7	5.17	0.40

3.3. Photoreactivity of α-ketoesters *via* photo-DSC

An elegant method to investigate the photoreactivity of the synthesized α-ketoesters is the use of photo-differential scanning calorimetry (photo-DSC). We chose to evaluate the photoreactivity of KE1–KE4 in three different resins, including 1,6-hexanediol diacrylate (HDDA), an equimolar mixture of urethane dimethacrylate and 1,10-decandiol dimethacrylate (DMM), and an aqueous hydrogel system comprised of 50 wt% polyethylene glycol diacrylate ($M_w \sim 700$ g mol^{-1}) in water (Fig. 5).

3.3.1. Photoreactivity using a broadband UV light source (320–500 nm). To compare the ability of cross-chain H-abstraction of the synthesized ketoesters, 2 mol% of ketoester moieties were dissolved in the respective monomers. Thus, regardless of the used PI, the same amount of radical-generating species was analyzed (*e.g.*, 2 mol% KE1, 2/3 mol% KE3). Thus, 2 functional group mol% (FG%) were used herein. Although ketoester-derived PIs work *via* the Norrish type II mechanism, no additional amine co-initiator was added to specifically focus on the intramolecular H-abstraction (Fig. 1). For organic-based formulations, BP/MDEA

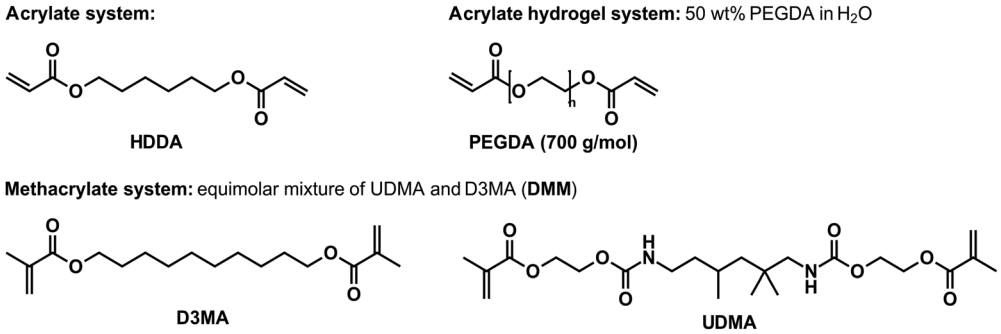

Fig. 5 Overview of monomers used in the photo-DSC study: hexanediol diacrylate (HDDA), an equimolar mixture of urethane dimethacrylate (UDMA) and decandiol diacrylate (D3MA) = dimethacrylate mixture (DMM), and a 50 wt% aqueous solution of polyethylene glycol diacrylate ($M_W \sim 700$ g mol^{-1}).

was used as a reference, whereas IC2959 was used as a reference water-soluble PI equimolar to KE1 (Fig. 3). All measurements were performed at 25 °C using a broadband UV lamp (320–500 nm) with a light intensity of 42 mW cm^{-2} on the sample surface.

Herein, three critical values were used to evaluate the photoreactivity of PIs in monomers. At first, the maximum rate of polymerization (R_p) relates to the curing speed and thus, higher values indicate higher reactivity. Additionally, the time until reaching the highest exotherm (t_{max}) was determined. Low t_{max} values imply high photoreactivity (Fig. 6). The double bond conversion was determined as the ratio of the experimentally measured heat of polymerization *via* DSC to the theoretical heat of polymerization of the vinyl system (Fig. S8 and Tables S4–S6).

The α-ketoester compounds KE1–KE3 outperform the reference BP + MDEA in both HDDA and DMM (Fig. 6(A) and (B)) with higher R_p and lower t_{max} values. Additionally, monomer conversions of >68% and >50% were determined in HDDA and DMM, respectively. Hence, the DBC is higher for KE1–KE3 compared to BP + MEDA (Tables S4 and S5). Thus, making KE2 and KE3 valuable alternatives for the state-of-the-art BP + MDEA system, without the need to add toxic amine co-initiators. Interestingly, the rate of polymerization increases in both monomers from KE1 (HDDA: 140 mmol L^{-1} s^{-1}, DMM: 29 mmol L^{-1} s^{-1})

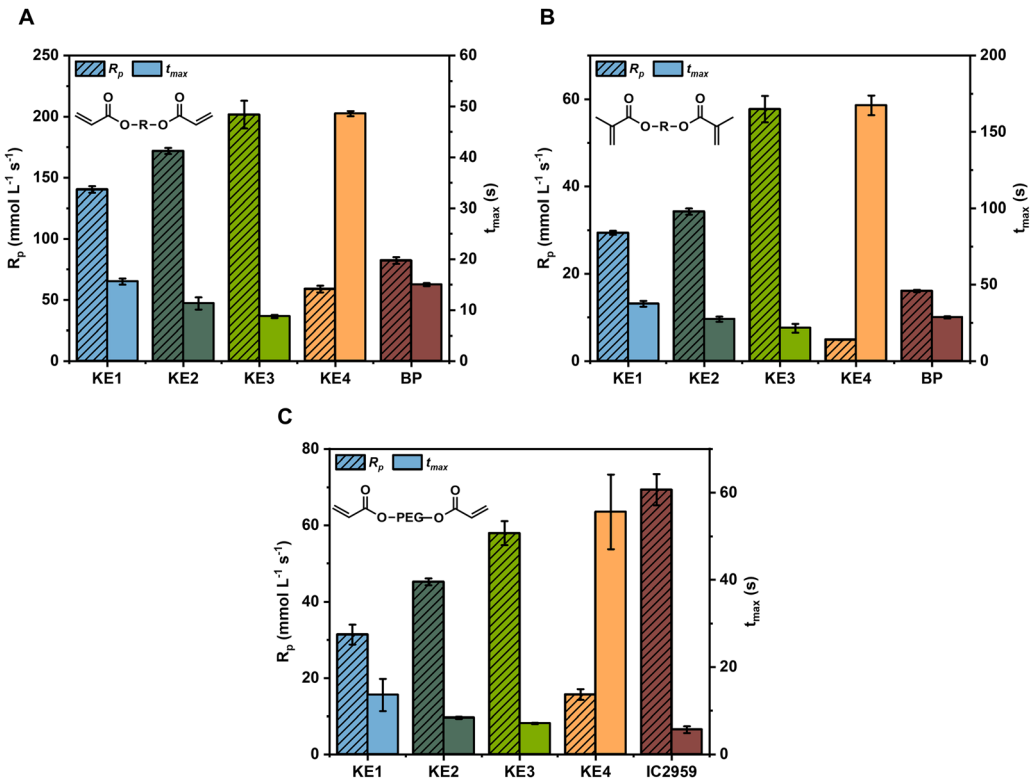

Fig. 6 Summarized results of the photo-DSC analysis: rate of polymerization R_p (dashed columns) and time until reaching the peak maximum t_{max} (filled columns) of 2 FG% of initiators measured in (A) HDDA, (B) DMM, and (C) 50 wt% PEGDA in water. Irradiation: broadband UV lamp (320–500 nm) @42 mW cm^{-2} on the sample surface.

to KE2 (HDDA: 172 mmol L^{-1} s^{-1}, DMM: 35 mmol L^{-1} s^{-1}) to KE3 (HDDA: 202 mmol L^{-1} s^{-1}, DMM: 58 mmol L^{-1} s^{-1}). A similar reduction in the t_{max} was observed for KE3 (HDDA: 9 s, DMM: 21 s) and KE2 (HDDA: 11 s, DMM: 27 s) compared to KE1 (HDDA: 16 s, DMM: 37 s). The increase of ketoester groups per molecule thus increases the photoreactivity, although an equimolar amount of radical-generating groups is present within the formulations. Thereby, higher photoreactivity may result from the proposed ''cross-chain'' H-abstraction in crowded molecules such as KE3. By contrast, upon incorporation of oligomeric ethylene glycol spacer groups to the pentaerythritol core (KE4), a decrease in photoreactivity in all tested monomer systems was observed. Thus, a close spatial vicinity of the ketoester groups is necessary to facilitate the H-abstraction over the arms of the PIs. Additionally, the higher molecular weight of KE4 decreases the radical mobility and thus contributes to a decrease in the overall reactivity. Additionally, conversion over time plots (Fig. S16A, B and Tables S13, S14) have been recorded using real time near infrared spectroscopy (RT-NIR) to further investigate the photoreactivity of the best performing KE1–3. Therein, high final DBC of ~85% (HDDA) and ~65% (DMM), respectively, were recorded for the ketoester-based PIs as well as for the reference BP + MDEA. Interestingly, higher slopes of the DBC over time (HDDA: 5.0–9.2% s^{-1}, DMM: 1.1–1.6% s^{-1}) were calculated for KE1–3 compared to the reference in both monomers (HDDA: 3.5% s^{-1}, DMM: 0.8% s^{-1}), indicating an enhanced rate of polymerization with increasing number of ketoester groups, corresponding to the previous findings made during photo-DSC analysis. However, an increase in the induction times (HDDA: 15–19 s, DMM: 37–45 s) was recorded for the ketoester-based systems compared to the references.

Interestingly, the shortest t_{max} values (<10 s) were found for ketoester PIs KE1–KE3 in aqueous PEGDA solutions (Fig. 6(C)). Similar to HDDA and DMM, KE4 showed generally decreased photoreactivity. Herein, the best-performing KE3 (t_{max}: 7.1 s) could even compete with the type I IC2959 (t_{max}: 5.7 s). Of course, the monomer PEGDA (M_n ~700 g mol^{-1}) offers easily abstractable protons that seem to further enhance the radical generation in ketoester PI-based systems. As already shown for bulk (meth)acrylates, the rate of polymerization increases with the amount of ketoester groups per molecule (KE1: 31 mmol L^{-1} s^{-1}, KE2: 45 mmol L^{-1} s^{-1}, KE3: 58 mmol L^{-1} s^{-1}), indicating beneficial curing behavior of crowded, multifunctional PIs also in aqueous systems. Near quantitative monomer conversions of >97% were observed (Table S6) for KE1–KE3 as well as IC2959. This is particularly interesting for biomedical applications, where high monomer conversions are required to exclude migration of unreacted monomers or PIs out of the cured resin.[40] Also for hydrogels, RT-NIR was used to assess the double bond conversion in real time (Fig. S16C and Table S15). Similar to the photo-DSC analysis, quantitative conversions were found for all tested systems, paired with increasing slopes of the DBC (3.74–4.06% s^{-1}) with an increase in ketoester groups. Low induction times of <10 s highlight the high photoreactivity of KE1–3 in aqueous-based formulations.

3.3.2. Enhancing the photoreactivity *via* type II co-initiators. Although the neat ketoester-based PIs exhibited high photoreactivity in (meth-)acrylate monomers, we aimed to further enhance their reactivity by the addition of type II co-initiators. Thereby, the mechanism is altered towards a bimolecular photoinitiating system comprised of the photoactive moiety and H-donors such as amines and ethers.[41] However, Gauss *et al.* reported the decomposition of commercially available ketoesters upon addition of aliphatic amines such as MDEA.[21] Furthermore, adding a strong base might lead to aldol condensation of ketoesters and thus deactivation of the photoreactive moieties (Fig. S15). By contrast, the basicity of aromatic amines such as ethyl-4-dimethylaminobenzoate (EDB, pK_A = 3[42]) is significantly lower compared to MDEA (pK_A = 9[43]). To circumvent base-catalyzed deactivation of the PIs, we added EDB as an amine co-initiator, which is frequently used as the co-initiator for camphor quinone in dental materials.[44] Additionally, (poly)ethers including poly(ethylene glycol) (PEG, 1 kDa) and poly(propylene glycol) (PPG, 725 g mol^{-1}) were chosen due to their lower toxicity compared to amines.[41] Herein, equimolar ratios (in respect to the ketoester moieties of the PI) of all co-initiators were added to the previously established best-performing KE3 (2 FG%) in both HDDA and DMM and photo-DSC was used to assess the photoreactivity at 25 °C with a broadband UV light source (320–500 nm, 40 mW cm^{-2}, Fig. S9).

As expected, the addition of the aliphatic MDEA to KE3 led to a decrease in photoreactivity for both HDDA (t_{max} > 20 s, R_p < 100 mmol L^{-1} s^{-1}, Fig. 7(A) and Table S7) and DMM (t_{max} > 60 s, R_p < 10 mmol L^{-1} s^{-1}, Fig. 7(B) and Table S8). Interestingly, the addition of MDEA to KE3-containing formulations resulted in turbid formulations. However, formulations without KE3 remained transparent, thus indicating either decomposition or aldol condensation of the PI under basic conditions. By contrast, the addition of the less basic aromatic amine EDB resulted in an increase in photoreactivity for KE3 in HDDA (t_{max}: 7.7 s, R_p: 243 mmol L^{-1} s^{-1}) while its addition to the methacrylate formulation (DMM) only marginally decreased the initiation efficiency. However, the addition of EDB increased the monomer conversion to >70% and >65% in HDDA and DMM, respectively. Interestingly, poly(ethers) enhanced the photopolymerization of KE3 in (meth)acrylates even more. Both PEG and PPG acted as powerful H-donors for KE3 in HDDA, resulting in t_{max} < 6.4 s and R_p of up to 350 mmol L^{-1} s^{-1}. Similar behavior was observed for DMM, as the t_{max} could be reduced to 16.7 s (KE3 + PPG) while increasing the R_p to 78.4 mmol L^{-1} s^{-1}. Thus, biocompatible poly(ether) co-initiators improved the photoreactivity of the best-performing KE3 in organic (meth)acrylates by additionally enhancing the H-abstraction required for the radical generation.

3.3.3. Photoreactivity using 385 nm LED. Generally, the use of light-emitting diodes (LEDs) offers multiple advantages compared to traditional mercury lamps, including higher safety, environmental responsibility, accompanied by higher energy efficiency and superior effectiveness.[18] Therefore, photo-DSC measurements of neat KE1–KE4 in HDDA, DMM, and

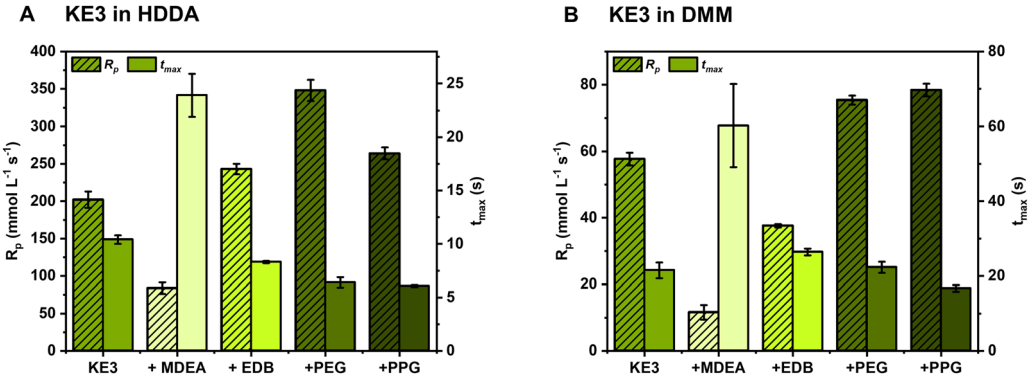

Fig. 7 Summarized results of the photo-DSC analysis: rate of polymerization R_p (dashed columns) and time until reaching the peak maximum t_{max} (filled columns) of 2 FG% KE3 + equimolar amounts of co-initiators MDEA, EDB, PEG, and PPG in (A) HDDA and (B) DMM. Irradiation: broadband UV lamp (320–500 nm) @42 mW cm^{-2} on the sample surface.

hydrogels were conducted using a 385 nm LED as light source (40 mW cm^{-2}, 25 °C). It has to be noted that all tested PIs show low molar extinction coefficients (<0.6 L mol^{-1} cm^{-1}, Table 1). However, low ε values do not necessarily imply lower photoinitiation efficiencies[18] and are accompanied by more homogeneous light penetration and higher curing depth, which is important, *e.g.*, for 3D printing.[45] Generally, the same trends as discussed for the broadband UV source were determined (Fig. 8, Fig. S10 and Tables S9–S11). With an increasing amount of ketoester moieties (KE1–KE3), higher photoreactivity was observed in HDDA, DMM, and PEGDA/water (50:50 wt%). Overall, KE1–KE3 outperformed BP + MDEA in both HDDA and DMM with low t_{max} (HDDA <12 s, DMM <28 s) and high R_p (up to 286 mmol L^{-1} s^{-1} for HDDA, 58 mmol L^{-1} s^{-1} for DMM). In the hydrogel system, KE1–KE3 showed significantly higher photoreactivity (KE3: t_{max} < 9 s, R_p: 56 mmol L^{-1} s^{-1}) compared to IC2959 (t_{max}: 19.5 s, R_p: 31 mmol L^{-1} s^{-1}) while maintaining high monomer conversions. However, the commercial reference shows no absorbance over 350 nm (Fig. S11), attributing to lower reactivity. Thus, the ketoester PIs demonstrated especially beneficial curing behavior when using a 385 nm LED compared in both organic and aqueous systems.

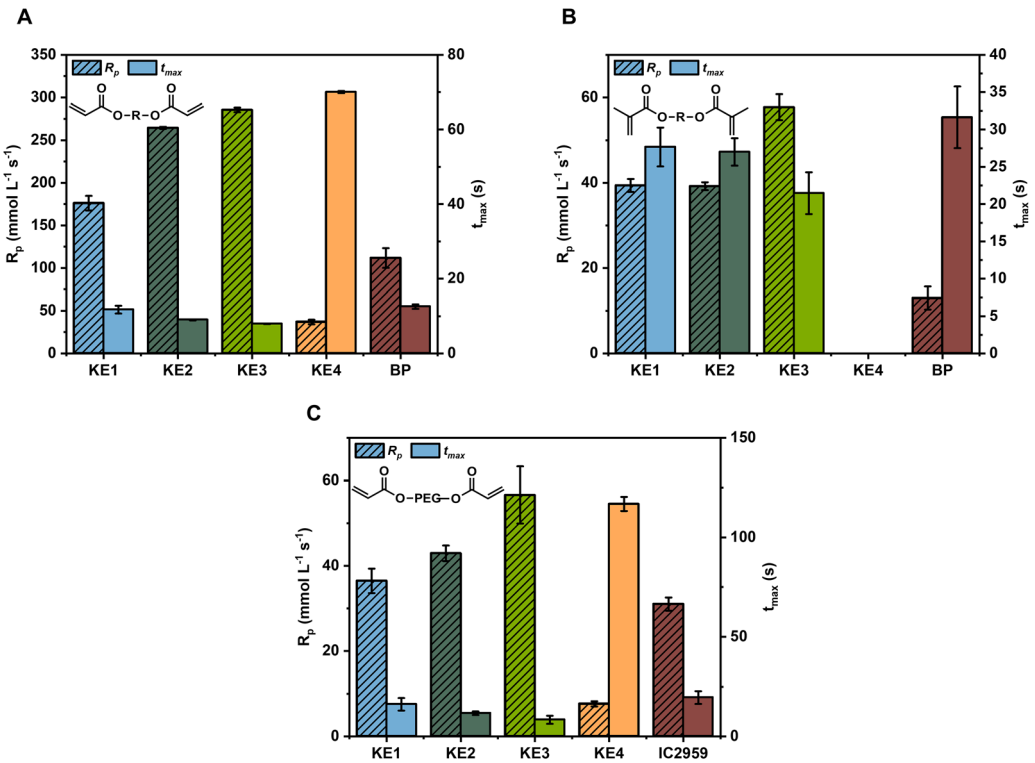

Fig. 8 Summarized results of the photo-DSC analysis: rate of polymerization R_p (dashed columns) and time until reaching the peak maximum t_{max} (filled columns) of 2 FG% of initiators measured in (A) HDDA, (B) DMM and (C) 50 wt% PEGDA in water. Irradiation: 385 nm LED @40 mW cm^{-2} on the sample surface.

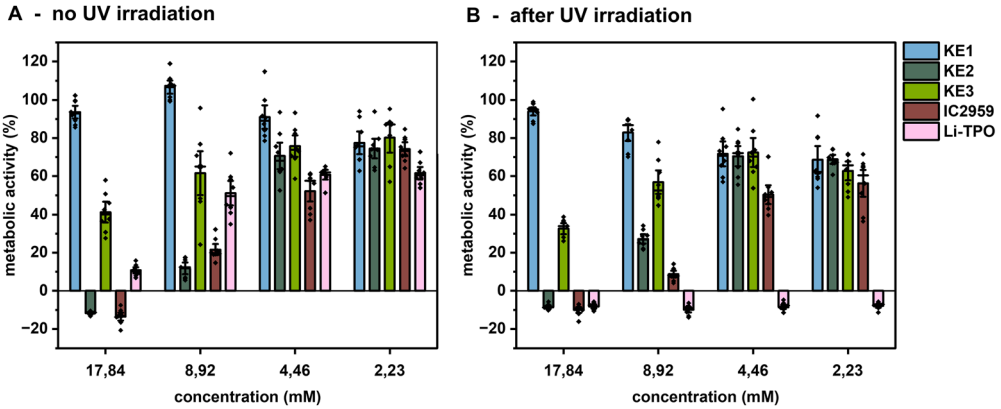

Fig. 9 Metabolic activity in % of L929 mouse fibroblasts after 24 h incubation with photoinitiator solutions either without (A) or with (B) 10 min of irradiation at 254 nm. KE1, KE2, KE3, IC2959, and Li-TPO were tested in concentrations of 17.84–2.23 mM diluted in the cell culture medium DMEM.

3.4. Evaluation of *in vitro* cytotoxicity

Besides sufficient photoreactivity, high biocompatibility is of utmost importance during PI development. Therefore, the cell viability of the best-performing KE1, KE2, and KE3 was determined with L929 mouse fibroblasts *via* a Presto Blue™ Assay. As references, the commercially available PIs IC2959 as well as the phosphine oxide Li-TPO were used due to their water solubility. Equimolar stock solutions of all PIs were prepared in DMEM (Dulbecco's Modified Eagle Medium) and standardized to a 40 mg mL^{-1} (17.48 mM) solution of IC2959 and adjusted with DMEM to obtain the PIs in final concentrations of 8.92 mM, 4.46 mM, and 2.23 mM. The solutions were either used directly (non-irradiated) or after 10 min of UV irradiation (254 nm) to generate photodecomposition products.

As expected from previous studies, KE1 exhibited excellent cell viability, as its metabolic activity was >80% for all tested concentrations (Fig. 9(A)).[21] This behavior was also visible after UV irradiation (Fig. 9(B)). For KE2, good cell viability (>70%) was obtained for concentrations from 4.46 mM and lower in both irradiated (Fig. 9(A)) and non-irradiated states (Fig. 9(B)). Interestingly, KE3 showed similar cell viability before and after irradiation (≥60% for ≤8.92 mM) and generally higher viability for high concentrations compared to KE2. Compared to the references IC2959 and Li-TPO, KE1 and KE3 showed better cell compatibility in all tested concentrations. IC2959 can be considered biocompatible at 4.46 mM and lower with and without UV irradiation.[46] However, irradiated solutions of Li-TPO resulted in no cell viability after 24 h. Interestingly, even at the highest PI concentration of 17.84 and 8.92 mM, respectively, the aliphatic α-ketoesters KE1 and KE3 showed metabolic activity of >50% demonstrating their great potential as biocompatible photoinitiators.

3.5. UV-Nanoimprint lithography

Resulting from its low toxicity and high photoreactivity, KE3 was applied in UV-nanoimprint lithography (UV-NIL). UV-NIL is known for its versatile applications, including the rapid production of microfluidic devices with high purity and high yield.[47–49] Thereby, micro- and nanostructured surfaces can be generated. Herein, KE3 was used as a low-toxic photoinitiator in resins containing bio-based acrylate monomers in a manual UV-NIL setup (Fig. S12). These manual UV-NIL tests were applied as preliminary feasibility tests for possible applications of KE3 in roll-to-roll UV-NIL pilot lines[50] that will allow high-volume manufacturing in the future. To facilitate the transfer into pre-industrial applications, the PI was used in 1 wt% (equal to 3 FG% for the acrylic hydrogel and 2.5 FG% for the aliphatic acrylate) in two acrylate-based resins with high bio-renewable content. Preliminary photo-DSC studies showed that KE3 exhibited excellent photoreactivity in both resins, with t_{max} of 8.5 s for the aliphatic diacrylate (JR NILcure bio-20) and t_{max} of 6.9 s for the hydrogel system (50 wt% M286 in water) (Fig. S13). For UV-NIL experiments, a thin layer of liquid resin was polymerized between a Si master stamp and a transparent polymer film *via* a 365 nm LED (20 s, 100 mW cm^{-2}). Thereafter, scanning electron microscopy (SEM) was used to visualize the nanoimprinted features in high resolution (Fig. 10).

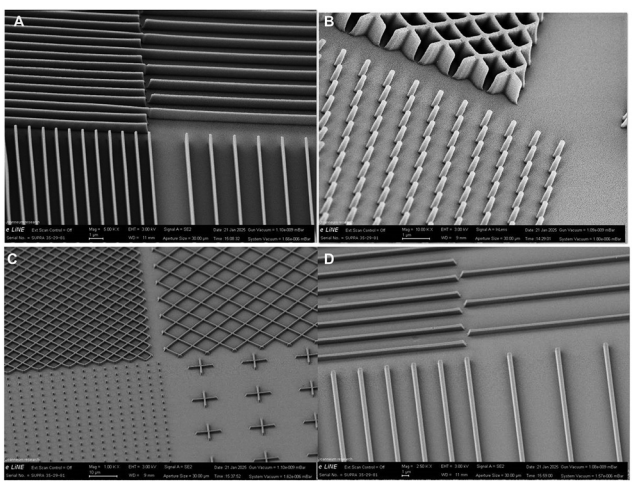

Fig. 10 SEM images of imprinted structures *via* UV-NIL. (A) and (B): resin JR NILcure (aliphatic diacrylate) containing 1 wt% KE3 as PI and (C), (D): hydrogel (50 wt% M286 in water) containing 1 wt% KE3 as PI.

For the aliphatic diacrylate, test structures of 200 nm width and 1 μm height could be reproduced. The fabricated structures ranged from simple straight lines to rhomboid structures and nanometer pins (line/space ratio = 1 : 8–1 : 1.5) (Fig. 10(A) and (B)). Similar conclusions can be drawn for the hydrogel samples (Fig. 10(C) and (D)). Due to the higher softness of the materials, the smallest dimensions of the hydrogel structures were 800 nm width (1 μm height). Still, very delicate structures, including straight lines (line/space ratio = 1 : 8–1 : 2), dots and crossed grids (line/space ratio = 1 : 4 and 1 : 2), could be transferred onto the substrates. The homogeneity and high fidelity of the imprinted patterns prove the excellent applicability of KE3 for future applications as a photoinitiator for large-scale roll-to-roll UV-NIL manufacturing.

3.6. DLP 3D printing

To further broaden the application scope of aliphatic α-ketoester-based photoinitiators, 3D printing of KE3 in various monomers was conducted. Similar to previous photo-DSC studies, a concentration of 2 FG% KE3 in acrylate and hydrogel formulations (50 wt% PEGDA in water) was chosen. First proof-of-concept printing tests using neat HDDA as monomer were conducted on a digital light processing (DLP) 3D printer (BP10 prototype, TU Wien) using a 385 nm LED light engine.[51] A layer thickness of 50 μm, light intensity of 60 mW cm^{-2} and an irradiation time of 10 s per layer were chosen after preliminary light exposure tests (Fig. S14A–C). Simple objects, including a pyramid with a square base of 1 × 1 cm^2 (Fig. S14D–F) and a hollow pyramid (square base of 8 × 8 mm^2, Fig. S14G) were fabricated. Even more delicate structures, including a boat (2 × 2 cm^2, Fig. S14H–I), could be printed with high dimensional fidelity. However, the brittle nature of HDDA prevented the successful removal of the fabricated parts. To counteract the poor mechanical properties of HDDA, we chose to continue with ethoxylated trimethylolpropane triacrylate (TMPTA, 912 g mol^{-1}), as KE3 exhibited sufficient photoreactivity therein (Table S12). Furthermore, ethers proved to be beneficial as H-donors during radical generation. To further enhance the printing resolution, the absorber quinoline yellow (QY) was added. Therefore, the printed parts exhibited a yellow color compared to the colorless, transparent polymer samples obtained from neat KE3 in *e.g.*, HDDA. Thus, a square pyramid object (1 × 1 cm^2) and a hollow square pyramid (1 × 1 cm^2) were fabricated with high resolution (Fig. 11(A)–(H)). SEM measurements revealed good interlayer adhesion and no signs of overpolymerization, resulting from the high selectivity of the photocuring reaction. Finally, successful 3D fabrication of hydrogels using KE3 as photoinitiator was achieved. The hydrogel prepolymer formulations contained

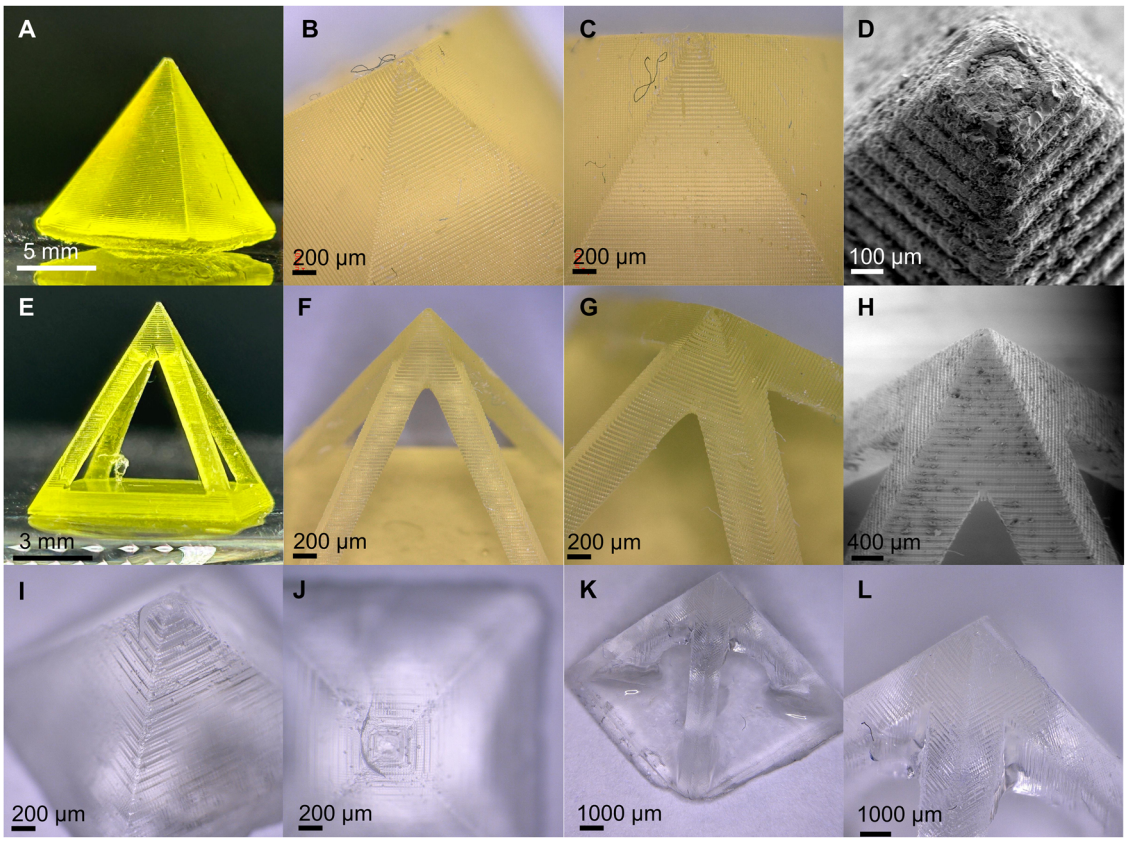

Fig. 11 Light-(LM) and scanning electron microscopic (SEM) images of structures printed of 2 FG% KE3 in various monomers. (A)–(C) LM and (D) SEM of square pyramids (2 FG% KE3 in ethoxylated TMPTA + 0.02 wt% QY), (E)–(G) LM and (H) SEM of hollow square pyramids (2 FG% KE3 in ethoxylated TMPTA + 0.02 wt% QY). LM images of 3D structures of hydrogels (2 FG% KE3 in 50 wt% aqueous PEGDA): (I) and (J) square pyramid and (K) and (L) hollow square pyramid.

PEGDA ($\sim$700 g mol^{-1}) as reactive monomer, as it is frequently used to fabricate functional biomaterials.[52,53] Even the addition of 50 wt% water as nonreactive diluent did not impair the high photoreactivity of KE3. Again, filled and hollow square pyramids (1 × 1 cm^2, Fig. 11(I)–(L)) were produced with excellent interlaminar attachment. To keep the resin as simple and biocompatible as possible, no UV absorber was added. Thereby, fully colorless and transparent biomaterials were produced. Although no signs of overpolymerization were observed, the high penetration depth of UV-light into transparent materials, lacking of sufficient UV absorbance, resulted in slightly enhanced dimensions compared to the original CAD design.[53,54] Still, the high photoreactivity and resolution prove the applicability of KE3 for future fabrication of more complex structures, for *e.g.*, tissue engineering applications.

4. Conclusions

In this study, we explored the synthesis of three fully aliphatic Norrish type II photoinitiators KE2-KE4 by systematically equipping inexpensive polyol starting materials with 2–4 ketoester groups. The obtained multifunctional ketoester derivatives exhibit absorption up to 400 nm, although they lack benzoyl chromophores. All synthesized compounds show excellent solubility in both organic and aqueous media and can thereby be used for a broad range of monomers. We demonstrated high photoreactivity of the synthesized compounds for free radical polymerization of (meth)acrylate monomers in bulk as well as in aqueous hydrogel systems upon irradiation with broadband (320–500 nm) and monochromatic LED light sources. By introducing evermore radical generating ketoester moieties, the initiation efficiency could be increased up to 3-times compared to the commercially available ethyl pyruvate (KE1) as shown by photo-DSC measurements. Moreover, KE2 and KE3 outperformed the state-of-the-art BP/amine system while exhibiting low cytotoxicity in the non-irradiated and irradiated state, respectively. Finally, the best performing KE3 was applied in UV-nanoimprint lithography and DLP-3D printing. High resolutions of 3D-structured objects on both the nanometer (UV-NIL) and macroscopic (DLP-3D printing) scale were shown without any signs of overpolymerization or discoloration of the produced parts. Thus, the developed aliphatic, biocompatible ketoester PIs show great potential in applications such as additive manufacturing or nanoimprinted microfluidic devices.

Author contributions

Antonella Fantoni: data curation, formal analysis, investigation, methodology, project administration, validation, visualization, writing – original draft, writing – review & editing. Judith Kraußß: data preparation, formal analysis, investigation, methodology, validation, writing – review & editing. Theresa Ammann: data preparation, formal analysis, investigation, methodology, validation, writing – review & editing. Philipp Melchior: data preparation, formal analysis, investigation, methodology, validation, writing – review & editing. Dieter Nees: conceptualization, formal analysis, funding acquisition, methodology, resources, writing – review & editing. Martin Frauenlob: conceptualization, formal analysis, funding acquisition, methodology, resources, writing – review & editing. Robert Liska: conceptualization, formal analysis, funding acquisition, methodology, project administration, resources, supervision, writing – review & editing. Stefan Baudis: conceptualization, data curation, formal analysis, investigation, methodology, project administration, supervision, validation, visualization, writing – review & editing.

Conflicts of interest

There are no conflicts to declare.

Data availability

The data supporting this article have been included as part of the supplementary information (SI). The SI contains NMR spectra of the synthesized compounds, further characterization of the compound KE4 (hydroxy value *via* 31P-NMR and gel permeation chromatographic (GPC) analysis), a chapter on the proposed photoinitiation mechanism, results of photo-DSC measurements at 320–500 nm with and without co-initiators, results of photo-DSC measurements at 385 nm, UV-Vis spectrum of the commercial photoinitiator IC2959, details on UV-nanoimprint lithography, details on DLP-3D printing, a chapter on the proposed mechanism of KE decomposition under basic conditions, and a real-time near infrared spectroscopic study of photopolymerization. Raw data for this article, beyond the scope of the SI, including raw data of all presented graphs, are available at TU Wien Research Data (**https://doi.org/10.48436/4pksk-8t382**). Supplementary information is available. See DOI: **https://doi.org/10.1039/d5ma00926j**.

Acknowledgements

The authors thank Dominik Laa and Jakob Ecker for their help with SEM and digital microscopy imaging of 3D printed samples. Funding by the Christian Doppler Research Association within the framework of a Christian Doppler Laboratory for ''Advanced Polymers for Biomaterials and 3D Printing'' and the financial support by the Austrian Federal Ministry of Economy, Energy and Tourism, and the National Foundation for Research, Technology is gratefully acknowledged. The authors acknowledge TU Wien Bibliothek for financial support through its Open Access Funding Program.

References

1 I. V. Khudyakov, *Prog. Org. Coat.*, 2018, **121**, 151–159.
2 M. Lee, R. Rizzo, F. Surman and M. Zenobi-Wong, *Chem. Rev.*, 2020, **120**, 10950–11027.
3 J. W. Stansbury, *J. Esthet. Restor. Den.t*, 2000, **12**, 300–308.

4 A. Bagheri and J. Jin, *ACS Appl. Polym. Mater.*, 2019, **1**, 593–611.
5 J. Zhou, X. Allonas, A. Ibrahim and X. Liu, *Prog. Polym. Sci.*, 2019, **99**, 101165.
6 S. M. Müller, S. Schlögl, T. Wiesner, M. Haas and T. Griesser, *ChemPhotoChem*, 2022, **6**, e202200091.
7 X. Ji, J. Liang, J. Liu, J. Shen, Y. Li, Y. Wang, C. Jing, S. A. Mabury and R. Liu, *Environ. Sci. Technol.*, 2023, **57**, 11704–11717.
8 Y. Nakagawa and K. Tayama, *Arch. Toxicol.*, 2002, **76**, 727–731.
9 IARC, IARC Monographs on the evaluation of carcinogenic risks to humans, International Agency for Research on Cancer, 2013.
10 ECHA, **https://echa.europa.eu/-/echa-adds-two-hazardous-chemicals-to-candidate-list**, (accessed 12.02.2024, 2024).
11 M. Popal, J. Volk, G. Leyhausen and W. Geurtsen, *Dent. Mater.*, 2018, **34**, 1783–1796.
12 X. Sun, X. He, M. Yi, S. Fan, B. Xiang, B. Yuan, J. Zhu, P. Luo, Y. Zou and Y. Pang, *Eur. Polym. J.*, 2024, **211**, 113025.
13 T. Gao, Z. Liu, J. Yin, J. Feng, C. Dietlin, F. Morlet-Savary, M. Schmitt, T. Petithory, L. Pieuchot, J. Zhang, F. Dumur, J. Lalevée and P. Xiao, *Angew. Chem., Int. Ed.*, 2025, **64**, e202425598.
14 J. Yin, Y. Zhang, B. Graff, C. Dietlin, M. Schmitt, F. Morlet-Savary, T. Petithory, L. Pieuchot, J. Zhang, Y. Xu, J.-M. Becht, J. Lalevée and P. Xiao, *Green Chem.*, 2025, **27**, 1451–1461.
15 W. Tomal, F. Petko, M. Galek, A. Świeży, M. Tyszka-Czochara, P. Środa, K. Mokrzyński and J. Ortyl, *Chem. Mater.*, 2024, **36**, 6421–6439.
16 A. Świeży, F. Petko, D. Krok-Janiszewska, P. Szymaszek, M. Galek and J. Ortyl, *Adv. Mater. Technol.*, 2025, **10**, 2402139.
17 S. Hu, X. Wu and D. C. Neckers, *Macromolecules*, 2000, **33**, 4030–4033.
18 T. Gao, Y. Zhang, F. Morlet-Savary, B. Graff, J. Zhang, P. Xiao, F. Dumur and J. Lalevée, *Small*, 2024, **20**, 2400234.
19 M. Yao, S. Liu, C. Huang, J. Nie and Y. He, *J. Photochem. Photobiol., A*, 2021, **419**, 113451.
20 E. Frick, H. A. Ernst, D. Voll, T. J. A. Wolf, A.-N. Unterreiner and C. Barner-Kowollik, *Polym. Chem.*, 2014, **5**, 5053–5068.
21 P. Gauss, M. Griesser, M. Markovic, A. Ovsianikov, G. Gescheidt, P. Knaack and R. Liska, *Macromolecules*, 2019, **52**, 2814–2821.
22 R. Taschner, P. Gauss, P. Knaack and R. Liska, *J. Polym. Sci.*, 2020, **58**, 242–253.
23 G. S. Hammond, P. A. Leermakers and N. J. Turro, *J. Am. Chem. Soc.*, 1961, **83**, 2395–2396.
24 P. A. Leermakers, P. C. Warren and G. F. Vesley, *J. Am. Chem. Soc.*, 1964, **86**, 1768–1771.
25 R. S. Davidson, D. Goodwin and P. F. de Violet, *Tetrahedron Lett.*, 1981, **22**, 2485–2486.
26 S. Rochat, C. Minardi, J.-Y. de Saint Laumer and A. Herrmann, *Helv. Chim. Acta*, 2000, **83**, 1645–1671.
27 F. A. Andersen, *Int. J. Toxicol.*, 1998, **17**, 1–241.
28 M. P. Fink, *Sepsis: New Insights, New Therapies*, 2006, pp. 147–159, DOI: **10.1002/9780470059593.ch10**.
29 M. P. Fink, *J. Intern. Med.*, 2007, **261**, 349–362.
30 X. Dai, J.-N. Hao, J. Gu and Y. Li, *ACS Appl. Bio Mater.*, 2020, **3**, 3792–3799.
31 Y. Xia Zhang, Y. He, Y. Liang, J. Tang, Y. Yang, H. Ming Song, M. Zrínyi and Y. Mei Chen, *Appl. Surf. Sci.*, 2023, **615**, 156328.
32 G. Theocharidis, H. Yuk, H. Roh, L. Wang, I. Mezghani, J. Wu, A. Kafanas, M. Contreras, B. Sumpio, Z. Li, E. Wang, L. Chen, C. F. Guo, N. Jayaswal, X.-L. Katopodi, N. Kalavros, C. S. Nabzdyk, I. S. Vlachos, A. Veves and X. Zhao, *Nat. Biomed. Eng.*, 2022, **6**, 1118–1133.
33 ECHA, **https://chem.echa.europa.eu/100.009.557/dossier-view/6017056a-5c9d-4963-9dac-4ebb9e89a33d/965a2b5e-f54e-4da7-ba14-e1944f2c8eda_2c6ccecf-87a7-44dc-b021-8fa04feb772a?searchText=ethyl%20pyruvate**, (accessed 04.02.2025).
34 C. Gorsche, K. Seidler, R. Harikrishna, M. Kury, T. Koch, N. Moszner and R. Liska, *Polymer*, 2018, **158**, 149–157.
35 Y. Pu, S. Cao and A. J. Ragauskas, *Energy Environ. Sci.*, 2011, **4**, 3154–3166.
36 J. Brandrup, *Polymer Handbook*, Wiley & Sons, New York, 4 edn, 1999.
37 C. Gorsche, M. Griesser, G. Gescheidt, N. Moszner and R. Liska, *Macromolecules*, 2014, **47**, 7327–7336.
38 D. Nees, S. Ruttloff, U. Palfinger and B. Stadlober, *Proc. SPIE*, 2016, **9777**, 46–63.
39 C. Dietlin, J. Lalevee, X. Allonas, J. P. Fouassier, M. Visconti, G. L. Bassi and G. Norcini, *J. Appl. Polym. Sci.*, 2008, **107**, 246–252.
40 A. Dureja, S. R. Acharya, S. Kini, A. Mayya and V. Hedge, *Eng. Proc.*, 2023, **59**(1), 160.
41 M. A. Tasdelen, N. Moszner and Y. Yagci, *Polym. Bull.*, 2009, **63**, 173–183.
42 J. D. Oxman, D. W. Jacobs, M. C. Trom, V. Sipani, B. Ficek and A. B. Scranton, *J. Polym. Sci., Part A: Polym. Chem.*, 2005, **43**, 1747–1756.
43 A. Tagiuri, M. Mohamedali and A. Henni, *J. Chem. Eng. Data*, 2016, **61**, 247–254.
44 H. Chen, M. Schmitt, B. Graff, F. Morlet-Savary, C. Hahn, H. Kelch, R. Maletz, A. Willner and J. Lalevée, *Macromol. Rapid Commun.*, 2024, **45**, 2400196.
45 G. A. Miller, L. Gou, V. Narayanan and A. B. Scranton, *J. Polym. Sci., Part A: Polym. Chem.*, 2002, **40**, 793–808.
46 I. O. f. Standardization, Biological evaluation of medical devices. Part 5: Tests for *in vitro* cytotoxicity, **https://www.iso.org/standard/36406.html**.
47 J. Chen, Y. Zhou, D. Wang, F. He, V. M. Rotello, K. R. Carter, J. J. Watkins and S. R. Nugen, *Lab Chip*, 2015, **15**, 3086–3094.
48 P. Toren, M. Smolka, A. Haase, U. Palfinger, D. Nees, S. Ruttloff, L. Kuna, C. Schaude, S. Jauk, M. Rumpler, B. Hierschlager, I. Katzmayr, M. Sonnleitner, M. W. Thesen, M. Lohse, M. Horn, W. Weigel, M. Strbac, G. Bijelic, S. Hemanth, N. Okulova, J. Kafka, S. Kostler, B. Stadlober and J. Hesse, *Lab Chip*, 2020, **20**, 4106–4117.
49 P. Toren, M. Rumpler, M. Smolka, A. Haase, S. Ruttloff, D. Nees, B. Stadlober, I. Katzmayr, B. Hierschlager, S. Kierstein, M. Sonnleitner, G. Bared, M. Horn, W. Weigel and J. Heese, *Eur. J. Mater. Sci. Eng.*, 2020, **5**, 11–16.

50 M. Leitgeb, D. Nees, S. Ruttloff, U. Palfinger, J. Götz, R. Liska, M. R. Belegratis and B. Stadlober, *ACS Nano*, 2016, **10**, 4926–4941.
51 F. Mayer, D. Laa, T. Koch, J. Stampfl, R. Liska and K. Ehrmann, *Mater. Horiz.*, 2025, **12**, 1494–1503.
52 D. Xue, J. Zhang, Y. Wang and D. Mei, *ACS Biomater. Sci. Eng.*, 2019, **5**, 4825–4833.
53 J. Wang, S. Stanic, A. A. Altun, M. Schwentenwein, K. Dietliker, L. Jin, J. Stampfl, S. Baudis, R. Liska and H. Grützmacher, *Chem. Commun.*, 2018, **54**, 920–923.
54 A. Urrios, C. Parra-Cabrera, N. Bhattacharjee, A. M. Gonzalez-Suarez, L. G. Rigat-Brugarolas, U. Nallapatti, J. Samitier, C. A. DeForest, F. Posas, J. L. Garcia-Cordero and A. Folch, *Lab Chip*, 2016, **16**, 2287–2294.